Hot Electron Relaxation Dynamics of Gold Nanoparticles Embedded in $MgSO_4$ Powder Compared To Solution: The Effect of the Surrounding Medium

Stephan Link,[†] Akihiro Furube,[‡,§] Mona B. Mohamed,[†] Tsuyoshi Asahi,[‡] Hiroshi Masuhara,[‡] and Mostafa A. El-Sayed*[,†]

Laser Dynamics Laboratory, School of Chemistry and Biochemistry, Georgia Institute of Technology, Atlanta, Georgia 30332-0400, and Department of Applied Physics, Osaka University, Suita, Osaka 565-0871, Japan

Received: August 27, 2001; In Final Form: November 19, 2001

To test the influence of the surrounding medium on the relaxation dynamics of the plasmon band bleach recovery of gold nanoparticles after excitation with femtosecond laser pulses, we embedded 14.5 and 12.1 nm colloidal gold nanoparticles (synthesized electrochemically) in $MgSO_4$ powder and investigated these samples by femtosecond diffuse reflectance spectroscopy. By measuring the relaxation dynamics over a wide range of excitation energies, we found that the fast decay component is slower by about a factor of 2 for the particles in the $MgSO_4$ powder compared to those in solution while no significant change in the slow decay component is observed. In agreement with this observation, we found that adding solvent to the particles embedded in the powder caused a decrease in the relaxation time from about 10 ps to 5 ps for the fast decay component. This leads to the conclusion that the electron−phonon relaxation in these gold nanoparticles depends on the chemical nature and/or physical phase (solid vs solution) of the surrounding medium. A discussion of this in terms of the type of phonon involved, and the nature of the electron−phonon and phonon−phonon relaxation processes is discussed. To our knowledge, this also presents the first time that a transient bleach could be observed by diffuse reflectance spectroscopy.

I. Introduction

Ultrafast dynamics of photoexcited noble metal nanoparticles is attracting great interest lately.[1−26] Many femtosecond pump−probe experiments of colloidal solution systems and of particles incorporated in optically transparent glasses have been carried out in order to investigate the relaxation processes of electrons with a non-Fermi distribution and the subsequent thermalization through electron−electron, electron−phonon, and phonon−phonon interactions. Most of the experimental effort has been devoted to the size[6,7,16,23,25,26] and shape[9] dependence of the electron−phonon coupling in small metal particles. Independent of the metal and its size and shape, it was found that the electron−phonon relaxation time increases with increasing excitation power in the high perturbation regime and a second, much longer decay component can then be observed.[5,7,14,15] This second component has been assigned to phonon−phonon relaxation between the metal particles and the surrounding medium and was found to be on the order of about 100 ps. For example, Hamanaka et al.[1] observed a decay of the plasmon band broadening of 6 nm silver nanoparticles with relaxation times of 2−3 and 200 ps. Perner et al.[2,3] measured relaxation times of 4 and 200 ps for 30 nm gold particles embedded in a sol−gel matrix after excitation at 400 nm. Inouye et al.[4] measured gold nanoparticles with a diameter of 7.6 nm in a SiO_2 glass matrix and found decay times of 2.8 and 120 ps. Ahmadi et al.[5−7] reported decay times of 2.5 and >50 ps for the electron−phonon and phonon−phonon relaxation times in 30 nm colloidal gold particles. Zhang and co-workers[10−13] observed slightly longer relaxation times of 7 and 400 ps for 15 nm gold nanoparticles in water when probed at 790 nm after excitation with 390 nm pulses. Furthermore, they reported a reduction of the decay times for the electron−phonon interactions from 7 to 3.5 ps when the solvent was changed from water to cyclohexane, suggesting that the electronic relaxation is sensitive to the surface environment. A similar dependence of the relaxation dynamics on the surrounding environment was found by Bigot and co-workers[18,19] for 6.5 nm silver nanoparticles. The electron−phonon relaxation increased from 0.77 to 1.4 ps when the matrix was changed from alumina to glass. This was explained in terms of the higher thermal conductivity of the alumina matrix.

Except for these two studies, the main focus of the ultrafast electron dynamics has so far mainly been on the size-dependence of the electron−phonon relaxation under low-intensity excitation conditions. Here we report on the electron cooling of gold nanoparticles in different media after high-intensity excitation with an amplified Ti:Sapphire laser. Under these conditions, the temperature change of the gold lattice is on the order of several tens of degrees. The transfer of the excitation energy to the surrounding medium, which acts as an energy sink, might therefore become an important factor in the observed relaxation dynamics, in contrast to the low excitation intensity experiments reported in the literature. We have therefore investigated the cooling dynamics of gold nanoparticles embedded in a $MgSO_4$ powder and compared the results with those obtained for the same particles in solution. This represents not only a change in the chemical nature of the surrounding species but also a change in the physical phase of the medium (liquid vs solid medium). We chose $MgSO_4$ powder as a surrounding medium because

* Corresponding author
[†] Georgia Institute of Technology.
[‡] Osaka University.
[§] Current address: Photoreaction Control Research Center, National Institute of Advanced Industrial Science and Technology.

10.1021/jp013311k CCC: $22.00
Published on Web 01/03/2002

we expected an even worse heat conduction for this medium compared to solution and much worse compared to a dielectric film. Since the conventional pump−probe transmission technique for transparent samples such as solutions and films cannot be applied to powder samples due to multiple light scattering, a time-resolved diffuse reflectance technique with a subpicosecond time resolution can be used instead to investigate ultrafast dynamics inside microcrystals or on solid surfaces. Since the $MgSO_4$ crystals are of micrometer size and therefore much larger than the 14.5 and 12.1 nm gold nanodots used in this study, it is reasonable to assume that the gold particles are mostly surrounded by air and to a lesser extent by the inorganic salt. In this paper, we compare the relaxation dynamics of gold nanodots in solution and embedded in $MgSO_4$ powder in order to determine if and how the particle interface may influence the relaxation dynamics after heating the electrons with a femtosecond laser pulse.

II. Experimental Techniques

Spherical gold nanoparticles were prepared by an electrochemical method.[27−29] In the electrochemical cell, a gold metal plate was used as the anode and a platinum plate as the cathode. Both electrodes were immersed in an electrolyte solution consisting of a cationic surfactant, tetraoctylammonium bromide (0.5 mol/L) dissolved in a mixture of acetonitrile and tetrahydrofuran (THF) with a volume ratio of 4:1. The electrolysis was carried out under ultrasonication with an applied current of 5 mA and at a temperature of 35 °C for about 30 min. The optical density was adjusted to about 0.8 at the plasmon absorption maximum in a 2 mm cuvette. Gold nanodots embedded in $MgSO_4$ powder were prepared from the colloidal solution by combining 8 mL of the freshly prepared solution with 20 g of $MgSO_4$ powder and drying this mixture in an oven at 200 °C. This yielded a homogeneous powder containing gold nanodots with a concentration of about 2.0 wt %. Two samples with mean sizes of 14.5 ± 4.5 and 12.1 ± 5.4 were synthesized for the studies presented here.

The size of the particles was analyzed by transmission electron microscopy (TEM) using a Hitachi HF-2000 field emission TEM operating at 200 kV after drying a drop of the colloidal solution on a carbon covered copper grid. From the TEM images, the size distribution was determined by counting at least 300 particles. UV−vis absorption spectra of the colloidal gold solutions were recorded on a Shimadzu UV-3101-PC spectrophotometer. Ground-state absorption spectra of the powder sample were evaluated by the Kubelka−Munk function:

$$\frac{K}{S} = \frac{(1-r)^2}{2r} \tag{1}$$

where K and S are the absorption and scattering coefficients and r is the diffuse reflectance. Here we measured the relative diffuse reflectance of the gold nanodots in $MgSO_4$ powder compared to MgO powder. The diffuse reflected light intensity was measured on a Hitachi F-4500 fluorescence spectrometer by scanning the wavelengths of incident and reflected light synchronously.

The femtosecond transient spectroscopy experiments were carried out as follows:[7] An amplified Ti:sapphire laser system (Clark MXR CPA 1000) was pumped by a diode-pumped, frequency-doubled Nd:Vandate laser (Coherent Verdi). This produced laser pulses of 100 fs duration (fwhm) with an energy of 1 mJ at 800 nm. The repetition rate was 1 kHz. A small part (4%) of the fundamental generated a white light continuum in a 1 mm sapphire plate, which was used as the probe light. The remaining laser light was split into two equal parts. One part was frequency-doubled in a BBO crystal to generate a 400 nm pump beam and the other part pumped an OPA (Quantronix TOPAS) which produced signal and idler waves with a total energy of 120 μJ. Tunable wavelengths in the visible range were then produced by SHG and SFG of the signal wave. The OPA was used if higher light intensities of the probe light were needed, which was the case for the diffuse reflectance measurements of the gold nanodots embedded in $MgSO_4$ powder. The excitation beam was modulated by an optical chopper (HMS 221) with a frequency of 500 Hz. The probe light was split into a signal and a reference beam. After passing the monochromator (Acton Research), both beams were detected by two photodiodes (Thorlab). The kinetic traces were obtained using a sample-and-hold unit and a lock-in-amplifier (Stanford Research Systems). The transient signals were recorded as the differential changes in the transmission $\Delta T/T$ and reflection $\Delta R/R$. For small values, this is approximately equal to the changes in the optical density ΔOD. The spot size of the excitation beam was about 600 μm, which was roughly 5 times larger than the probe pulse.

Time-resolved diffuse reflectance spectra[30,31] were collected on a second laser system consisting of a self-mode-locked Ti:sapphire laser (Coherent Mira 900 Basic) pumped by an Ar^+ laser (Coherent Innova 310) and a Ti:sapphire regenerative amplifier system (Continuum TR70) with a Q-switched Nd:YAG laser (Continuum Surelight I). The fundamental output from the regenerative amplifier (780 nm, 3−4 mJ/pulse, 10 Hz) was frequency doubled to regenerate 390 nm pump pulses. The average excitation energy was in the range of several tens of μJ with a spot size at the sample of about 2 mm. The residual of the fundamental output was focused into a quartz cell with a path length of 1 cm containing water to generate a white light continuum used as the probe pulse. The transient diffuse reflectance spectra were then recorded as a function of probe delay with a polychromator combined with a multichannel photodiode array and corrected for shot-to-shot spectral intensity fluctuation of the white light continuum by using another polychromator and multichannel photodiode array. Transient absorption intensity was displayed as percentage absorption (% absorption $= 100 \times (1 - R/R_0)$, where R and R_0 represent the intensities of the diffuse reflected light of the probe pulse with and without excitation, respectively).

III. Results

A. Steady-State Absorption Spectra of Gold Nanodots in Solution and in $MgSO_4$ Powder. Figure 1a shows a TEM image of the electrochemically prepared gold nanodots. The TEM image was taken after a drop of the diluted colloidal solution has been dried on a carbon covered copper TEM grid immediately after the synthesis. The average size of the gold nanodots is 14.5 ± 4.5 nm. The colloidal solution was found to be stable over the time period of the spectroscopic measurements (a few month). Furthermore, the photostability was checked by measuring the absorption spectrum before and after each laser experiment. An absorption spectrum of the colloidal solution is shown in Figure 1b (solid line). The plasmon resonance is located at 532 nm. While a size distribution of 30% for the electrochemically prepared nanodots is not quite as good as the one observed for gold nanodots prepared by chemical reduction with sodium citrate (~10%) in aqueous solution,[9] the electrochemical preparation method has two advantages. First, the concentration and therefore the optical

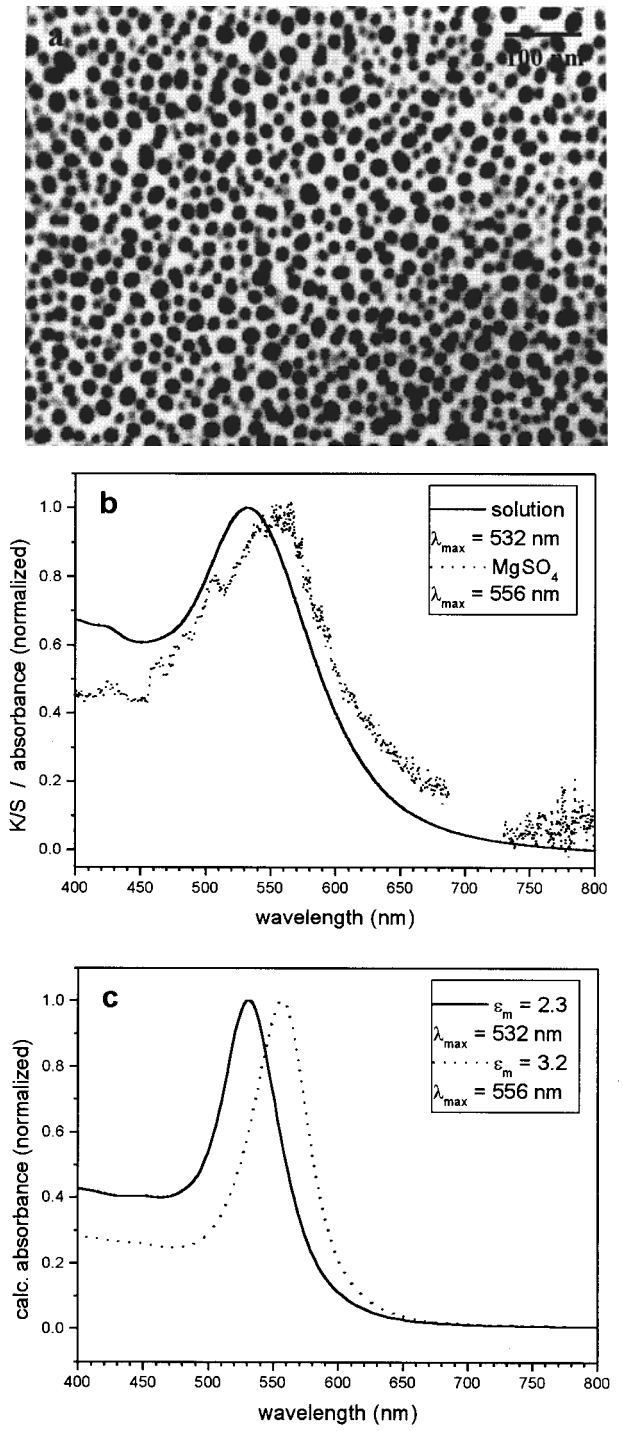

Figure 1. (a) TEM image of gold nanoparticles prepared electrochemically and taken after a drop of the colloidal solution has been evaporated on a carbon covered copper grid. A statistical analysis of the size distribution gives a mean particle diameter of 14.5 ± 4.5 nm. (b) Ground-state absorption spectra of the colloidal solution (solid line) and the gold particles embedded in $MgSO_4$ powder (dotted line). The plasmon absorption maximum is red-shifted from 532 to 556 nm due to a change in the medium dielectric constant when changing the environment from an organic solvent to an inorganic salt. The absence of a broad shoulder at the red edge of the plasmon absorption in the solid sample indicates that no significant aggregation has taken place when adding the $MgSO_4$ powder in agreement with X-ray data. In panel c, calculated plasmon absorption spectra are shown for two different values of the medium dielectric constant ϵ_m, which were chosen as to match the experimentally observed absorption maxima. Since $MgSO_4$ has indeed a larger dielectric constant than the solvent mixture used here, the shift of the plasmon absorption toward longer wavelength can be explained in terms of a change in ϵ_m due to a different particle environment.

density of the colloidal solution are much higher than the concentration of citrate stabilized gold particles. Second, the synthesis is carried out in a mixture of organic solvents (acetonitrile and THF) which can easily be mixed with $MgSO_4$ powder and then dried.

The ground-state absorption spectrum of the gold nanoparticles embedded in $MgSO_4$ powder is also shown in Figure 1b (dotted line). The maximum of the plasmon absorption is found at 556 nm and is red-shifted by 24 nm compared to the particles in solution. However, since no broad shoulder at the red edge of the plasmon resonance can be seen, an aggregation of the gold particles during the preparation of the gold nanodot-$MgSO_4$ composite can be excluded. Furthermore, X-ray studies carried out on the nanodots in $MgSO_4$ powder and on pure $MgSO_4$ powder show that (1) the line width of the diffraction peaks of the gold particles is in agreement with the average size determined from the TEM analysis of the colloidal solution and (2) there is no chemical interaction between the $MgSO_4$ and the gold particles as the position of the diffraction peaks for the $MgSO_4$ remained unchanged after the addition of the gold nanodots. An explanation for the red shift of the plasmon resonance upon changing the environment of the gold nanoparticles could be the higher dielectric constant of $MgSO_4$ compared to the mixture of organic solvents. Figure 1c shows two calculated absorption spectra for gold nanodots using the dipole approximation of the Mie theory:[32−34]

$$\sigma_{ext} = \frac{9V\epsilon m^{3/2}}{c} \frac{\omega\epsilon_2(\omega)}{[\epsilon_1(\omega) + 2\epsilon m]^2 + \epsilon_2(\omega)^2} \qquad (2)$$

where σ_{ext} is the extinction cross section, V is the spherical particle volume, c the speed of light, and ω the angular frequency of the exciting radiation. ϵ_m and $\epsilon(\omega) = \epsilon_1(\omega) + i\epsilon_2(\omega)$ denote the dielectric functions of the surrounding medium (assumed to be frequency-independent) and of the particle material, respectively. The data for the dielectric function of gold was taken from ref 35. The values for ϵ_m were chosen as to match the experimentally observed maxima of the plasmon resonance. No attempt, however, was made to account for the much broader line width of the plasmon band found in the experimental spectrum. The larger line width might be due to an inhomogeneous size distribution as well as to other broadening mechanisms described for particles in the intrinsic size range[32] (e.g., enhanced electron-surface scattering, chemical interface damping, etc). In conclusion, these simple calculations already show that the red shift of the surface plasmon resonance can be understood in terms of a change in the surrounding environment (as expressed by ϵ_m).

B. Time-Resolved Absorption Spectra of Gold Nanodots in $MgSO_4$ Powder. Figure 2 shows the transient diffuse reflectance spectra taken after different delay times. The excitation wavelength was 390 nm and the excitation power was 2.89 μJ/per pulse. The average size of the nanodots in these studies was 12.1 ± 5.4 nm. Although the positive absorption to the blue edge of the surface plasmon resonance is not as clearly resolved in the spectra shown in Figure 2 compared to earlier results obtained for the solution,[5−7] overall very similar features are found in the diffuse reflectance spectra for the nanodots in $MgSO_4$ powder with the strong bleach of the plasmon resonance and a positive absorption band at longer wavelength. For a better comparison, the ground-state absorption of the gold nanodots in $MgSO_4$ powder is also included in Figure 2 (dotted line), which clearly shows that the bleach maximum occurs at the same wavelength as the ground state absorption

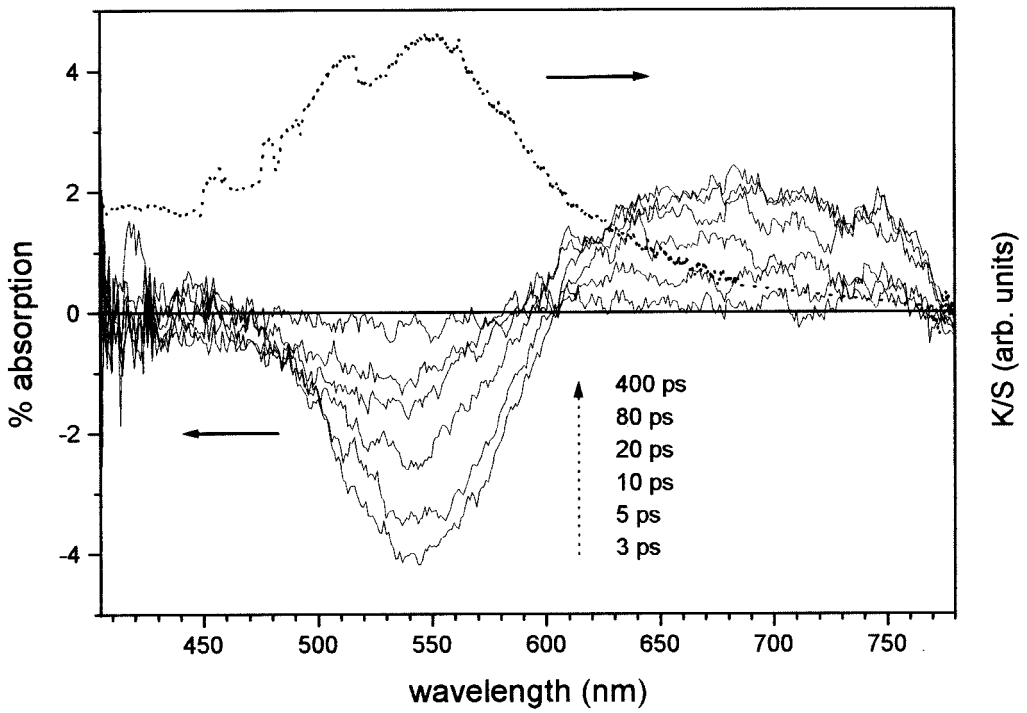

Figure 2. Ground state (dotted line) and transient diffuse reflectance spectra of gold nanoparticles embedded in $MgSO_4$ powder recorded at different delay times. The average diameter of the particles in this experiment was determined to be 12.1 ± 5.4 nm, and the excitation wavelength was 390 nm. The transient reflectance spectra are similar to those obtained earlier on colloidal gold solutions with a strong bleach centered at the maximum of the ground-state plasmon absorption.

maximum. The transient absorption has almost completely recovered after 400 ps. According to earlier experiments, the bleach recovery has been assigned to electron−phonon relaxation after the selective excitation of the electron gas followed by phonon−phonon interactions between the gold particles and the surrounding medium with relaxation times on the order of 1−4 ps and ∼100 ps, respectively.[1−26] With the knowledge of the ground-state and excited-state spectral features of the gold nanoparticles embedded in $MgSO_4$ powder, single-wavelength kinetics were carried out in order to investigate if the relaxation dynamics of the bleach spectrum are influenced by the environment. These studies were mainly carried out on a second sample with a slightly larger mean diameter of 14.5 nm (the absorption spectrum and TEM image of this sample have already been discussed in Figure 1) and are presented in the next section since more data are available for this particular sample. Single-wavelength kinetics obtained from the transient diffuse reflectance spectra in Figure 2 for the 12. 1 nm gold nanoparticles embedded in $MgSO_4$ powder and measured on one femtosecond system using a polychromator coupled to a multichannel photodiode array agree however very well with the direct measurements of the kinetic curves carried out on a second femtosecond system using a monochromator and photodiode setup combined with an lock-in amplifier. In addition, it should be mentioned that to our knowledge, this is the first time that a transient bleach has been recorded by diffuse reflectance spectroscopy. Monitoring a bleach with this method is usually complicated by the fact that the overall reflected light intensities are very small.

C. Comparison of the Bleach Recovery Dynamics between Solution and $MgSO_4$ Powder. Figure 3 shows four kinetic traces obtained for 14.5 nm gold particles in solution (a and c, recorded in a transmission geometry) and for the same particles in $MgSO_4$ powder (b and d, recorded in a diffuse reflectance geometry) at different excitation powers. The excitation wavelength was set to 400 nm in all cases, and the observation wavelength was 530 and 540 nm for the transmission and reflectance measurements, respectively. A wavelength close to the plasmon absorption maximum was chosen in order to achieve maximum sensitivity for the transient absorption signal (see also below). From Figure 3, it can be seen qualitatively that at low pump powers only one decay component is present which has previously been ascribed to the electron−phonon relaxation.[1−26] With increasing pump power, the fast decay component becomes longer, and a second much longer component is also present. The latter has been assigned to the phonon−phonon relaxation[1−16] between the hot particles and the surrounding medium. This trend is well-known for the metal nanoparticles in colloidal solution or in a transparent glass matrix.[1−16] The reason for the longer relaxation dynamics at higher pump intensities is the fact that the heat capacity of the electron gas is temperature dependent.[5,7,14,15] On the other hand, it could be argued that qualitatively a higher initial electron temperature caused by a more intense pump pulse will lead to a longer relaxation time because it will take the particle longer to cool to its initial temperature especially if the surrounding medium has a low heat conductivity. From the results in Figure 3, this trend of increasing relaxation times with increasing laser pump power is also observed for gold nanoparticles embedded in $MgSO_4$ powder and is hence independent of the specific medium and its phase (solution vs solid matrix). It should, however, be pointed out here that this behavior is true for the high perturbation regime which is examined in this paper, while at very low excitation powers the plasmon bleach recovers with an electron−phonon relaxation time which is independent of the laser pump power.[18−23] These experiments are usually performed with a higher repetition rate (100 MHz) unamplified femtosecond laser using a Ti:sapphire oscillator only. Since it is the aim of this study to investigate the role of the surrounding medium on the electron and lattice cooling after intense heating of the particles possibly inducing a bottleneck in the relaxation

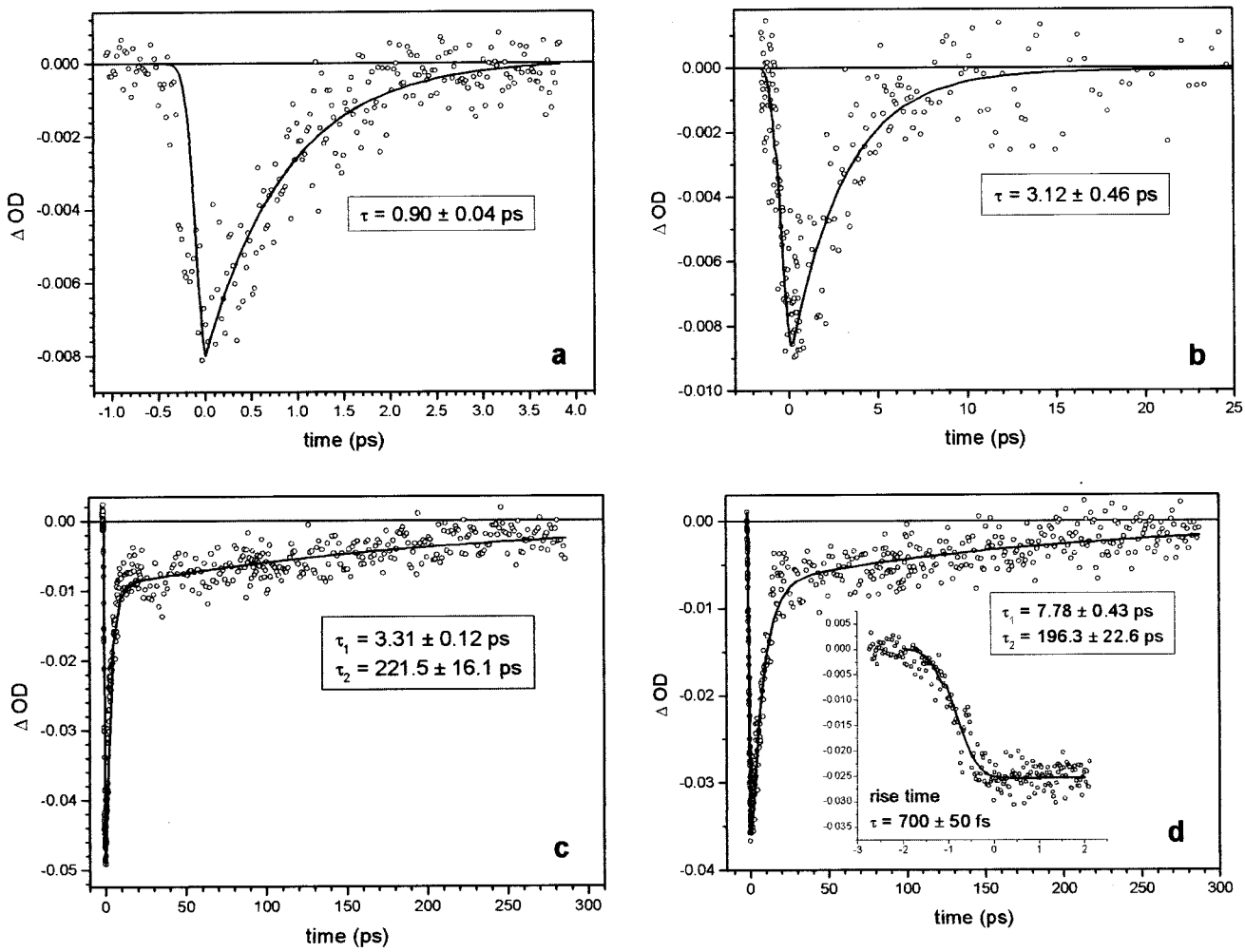

Figure 3. (a and c) Plasmon bleach recovery of 14.5 nm spherical gold nanoparticles in solution. Excitation was carried out at 400 nm, and the probe wavelength was set to 530 nm recording the transient transmission changes. The pump power was 10 nJ and 630 nJ for panels a and c, respectively. As the pump power increases from panel a to panel c, the relaxation time increases from 900 fs to 4.25 ps, while a slow decay component is also observed in panel c. (b and d) Plasmon bleach recovery of 14.5 nm spherical gold nanoparticles embedded in $MgSO_4$ powder. Excitation was carried out at 400 nm and the probe wavelength was set to 540 nm recording the transient changes in the diffuse reflectance. The pump power was 460 nJ and 2.22 μJ for panels b and d, respectively. Although the absolute value of the excitation pulse energy is considerably larger for the gold nanoparticles in $MgSO_4$ powder, the same trend of an increasing fast relaxation time with increasing pump intensity and the appearance of a slow decay component is also observed. The inset in panel d shows the rise of the plasmon band bleach on a shorter time scale. The rise can be reproduced by an instrumental response function with a width of 700 fs. This time is much longer than the pulse duration (100 fs) and also longer than the rise time for the transient transmission signals in panels a and c, which occur on the time scale of the excitation pulse. The slower rise of the plasmon band bleach for the gold nanodots in $MgSO_4$ powder is determined by the diffuse reflectance technique itself and reflects the finite penetration depth of the pump and probe pulses and the multiple scattering events along this distance.

dynamics, we take advantage of the higher pump intensities available from an amplified femtosecond system.

The kinetic traces in Figure 3a,b show the results obtained for the lowest possible excitation energy at which a bleach signal was still detectable with our setup. However, while the absolute maximum bleach intensities are very similar for both decay curves, the bleach recovery is longer by about a factor of 3 for the gold nanoparticles embedded in the $MgSO_4$ powder (3.12 ps vs 900 fs for the particles in $MgSO_4$ powder and solution, respectively). On the other hand, the excitation energy was 460 nJ for the particles in $MgSO_4$ powder in Figure 3b, which is much higher than the 10 nJ per pulse excitation energy used for the colloidal solution in Figure 3a. It could be argued that the longer relaxation time is simply due to a higher excitation energy. However this also leads to the following questions: (i) Are the sensitivity and the time-resolution of the transmission measurement different from the reflectance measurements? (ii) How much of the excitation energy was actually absorbed by the gold nanoparticles in $MgSO_4$ powder compared to the nanoparticles in solution? To answer the first question, we checked several factors, which will be discussed first.

1. Is There a Difference in the Sensitivity and Time-Resolution of the Two Setups? Concerning the time-resolution, the inset in Figure 3d shows the rise of the plasmon band bleach on a shorter time scale. The rise can be reproduced by an instrumental response function with a width of 700 fs. This time is much longer than the pulse duration (100 fs) and also longer than the rise time for the transient transmission signal in Figure 3a,c, which occurs on the time scale of the excitation pulse. The slower rise of the plasmon band bleach for the gold nanodots in $MgSO_4$ powder is determined by the diffuse reflectance technique itself and reflects a finite penetration depth of the pump and probe pulses and the multiple scattering events along this distance. However, the rise time of 700 fs is still shorter than the bleach recovery dynamics of 900 fs seen for the colloidal solution in Figure 3a, and it should therefore be possible to measure subpicosecond relaxation times with the diffuse reflectance setup. More importantly, simulations of the

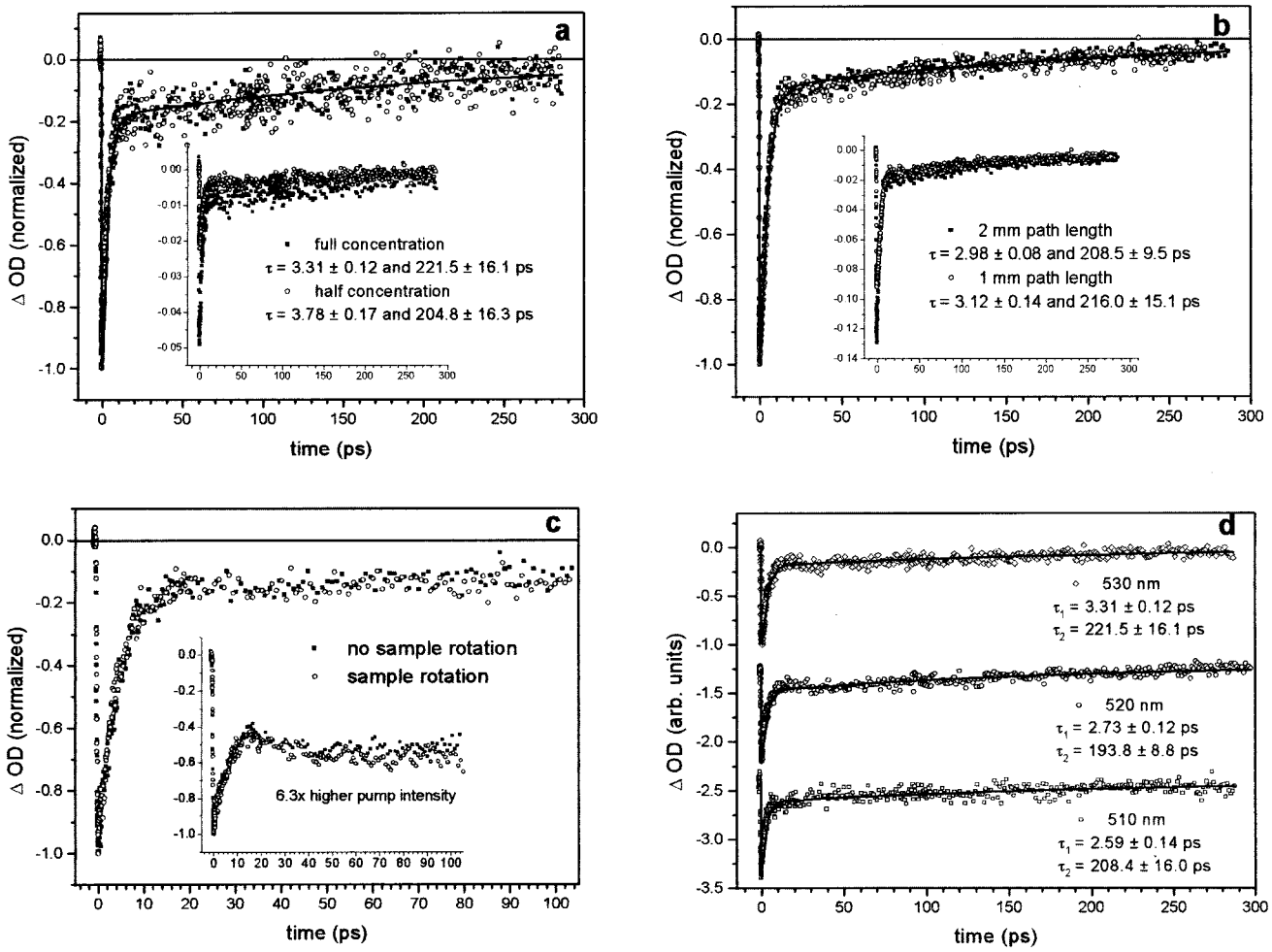

Figure 4. Effect of sample concentration on the plasmon bleach relaxation dynamics of 14.5 nm gold nanodots in solution. Excitation was carried out at 400 nm and the probe wavelength was set to 530 nm. The excitation power was 0.88 μJ. Although the total signal intensity is lower for a lower sample concentration (a) and for a shorter optical path length (b) (see insets), the relaxation dynamics are not changed which is clearly seen after normalization (main parts of panels a and b). Therefore, the sample concentration (a) and the total sample volume (b) when comparing optical cells with different path lengths have no effect on the cooling of the gold nanodots after femtosecond laser excitation. (c) Effect of sample rotation (open circles) compared to no rotation (solid squares) on the plasmon bleach relaxation dynamics of 14.5 nm gold nanodots in solution at 530 nm after excitation with 400 nm femtosecond pulses having a pulse energy of 0.21 μJ. For this pump power as well a for a 6.3 times higher pump power (see inset), no change in the relaxation dynamics can be seen. (For comparison, the traces in panel c have been normalized.) (d) Observation wavelength dependence of the plasmon bleach relaxation dynamics of 14.5 nm gold nanodots in solution. The excitation power was also 0.88 μJ. While the first component of the bleach relaxation becomes slightly faster for shorter observation wavelength, no significant change in the slow relaxation component can be seen considering the error in the decay times. This, however, cannot explain the differences seen in the relaxation dynamics for the gold nanodots in solution compared to the dots in $MgSO_4$ powder even if the probe wavelength of 540 nm is not exactly matching the plasmon band bleach maximum.

time-resolved diffuse reflectance have shown that the time resolution is mainly determined by the absorption coefficient.[30] For powder samples with a large absorption coefficient[30] ($K \geq 100$ cm^{-1}), subpicosecond time resolution is possible by diffuse reflectance spectroscopy. For 10 nm gold nanoparticles, one can estimate an absorption coefficient for the gold nanodot$-MgSO_4$ composite in the following way. The extinction coefficient of the colloidal solution is about 1×10^8 M^{-1}cm^{-1}, assuming an atomic extinction coefficient[9] of 4000 M^{-1}cm^{-1} and the fact that a 10 nm particle contains about 30000 atoms using the bulk density of gold (59 atom/nm^3). The concentration of the gold particles in the powder is about 0.9×10^{-5} mol/L because 2 wt % corresponds to 0.3 vol % using densities of 19 and 2.7 g/cm^3 for gold and $MgSO_4$, respectively, and a gold particle volume of 500 nm^3. Hence, the absorption coefficient is $K = 2.3 * 1 \times 10^8$ L mol^{-1} cm^{-1} $* 0.9 \times 10^{-5}$ mol/L $= 2 \times 10^3$ cm^{-1}. Therefore, subpicosecond time resolution is possible in these studies.

Concerning the sensitivity, the signal-to-noise ratio was generally better for the transmission experiments. The total bleach intensity however also depends on the actual concentration of the gold nanodots and the optical path length of the cell as shown in panels a and b, respectively, of Figure 4. The insets show the original data for comparison of the total signal intensities while in the main part the kinetic traces have been normalized in order to compare the effect of concentration (Figure 4a) and optical path length (Figure 4b) on the bleach recovery dynamics. The bleach intensity becomes larger for a larger number of excited gold nanoparticles as seen in the insets, but the overall relaxation dynamics are independent of the particle concentration. For the powder samples, a concentration of 2 wt. % of gold nanoparticles in $MgSO_4$ powder was found to be best for the diffuse reflectance measurements, which is much higher than that for the colloidal solution. However, the penetration depth of the excitation and probe pulse is much shorter as well so that a quantitative comparison is extremely

difficult. Since the relaxation dynamics are independent of concentration, it is justified to compare the dynamics of the two different samples while total bleach intensities are not meaningful.

Furthermore, we tested the influence of sample rotation on the relaxation dynamics of the solution sample as shown in Figure 4c. Sample rotation was usually carried out for the measurements of the particles in solution in order to ensure the excitation of different particles with each laser shot, but the powder samples could not be rotated. According to our studies, sample rotation has no effect on the bleach recovery dynamics, which was checked for different excitation powers. The inset of Figure 4c shows a comparison between sample rotation and no sample rotation for a 6.3 times higher energy of the 400 nm excitation pulse. Note that the plasmon band bleach first recovers and then starts to increase again at a delay time of about 20 ps. This was also reported by Hodak et al.[15] and was assigned to a change in the medium dielectric constant as the solvent's temperature increases, which in turn leads to a blue shift of the plasmon band. It is only observed at high excitation powers but is not unique to the transmission experiment. Since this increase complicates the data fitting and since the bleach recovery would then be mainly due to the cooling of the solvent around the particles, all experiments were carried out with excitation energies in a range where such an increase in the bleach intensity after 20 ps was not observed.

Finally, the dependence of the relaxation dynamics on the observation wavelength was also checked. The single-wavelength studies were carried out at 540 nm for the gold nanoparticles embedded in $MgS0_4$ powder, which is on the blue side of the bleach maximum (556 nm). This will contribute to the lower sensitivity. However, the probe light stability for our optical parametric amplifier was better at this wavelength than at the bleach maximum. The probe wavelength for the colloidal solution was set to 530 nm, which corresponds to the bleach maximum in this case. To exclude that any differences in the relaxation dynamics might simply be related to the probe wavelength, its dependence on the relaxation dynamics was studied for the colloidal solution and the results are shown in Figure 4d. While the fast relaxation component decreases slightly for shorter observation wavelength, no significant change in the slow relaxation time can be seen. This rather small dependence on the observation wavelength cannot explain the differences seen in the relaxation dynamics for the gold nanodots in solution compared to the dots in $MgSO_4$ powder even if the probe wavelength of 540 nm is not exactly matching the bleach maximum of the plasmon band. In fact, the off-center probe wavelength should give rise to a small decrease in the fast relaxation time for the dots in $MgSO_4$ powder. The opposite is however observed. In summary, we find no indication that the differences in the relaxation dynamics for the two systems studied here can be related to the two different experimental techniques.

2. How Much Laser Energy is Actually Absorbed by the Particles in the Two media? This depends on the absorption coefficient in both media. In principle, one would like to compare the relaxation dynamics of the gold nanodots in the different media after they have absorbed the same amount of laser energy and have therefore the same initial electron temperature. However, since the absorption cross section is dependent on the environment, as can be seen from Figure 1b,c, it is not justified to simply use the same total laser pulse energy as measured in front of the sample. One solution would be to correct the excitation pulse energy by the measured ground-state absorption spectra shown in Figure 1b. The Kabelka−Munk function gives the absorption coefficient K divided by the scattering coefficient S, and the latter also includes the scattering by the $MgSO_4$ powder, which furthermore is not a constant over the measured wavelength range and is not known in our case. Hence, extracting the true absorption coefficient of the gold nanodots in $MgSO_4$ powder is not possible. The fact that multiple scattering events are possible in the powder further complicates the determination of the exact amount of absorbed laser energy.

On the other hand, Hodak et al.[14−16] have used a different approach when comparing the relaxation dynamics of different size gold nanoparticles, irrespective of their absorption cross sections. They performed a series of measurements with varying excitation power and extrapolated the obtained relaxation times to zero pump power. They then compared the limiting lifetimes, which directly correspond to the electron−phonon relaxation time. This is done for all the data we measured during the course of this investigation, and the results are shown in Figure 5. Figure 5a summarizes the values obtained for the fast decay component, while in Figure 5b, the decay times of the slow component are plotted. The solid (open) symbols correspond to the measurements performed on gold nanodots in $MgSO_4$ powder (solution). As already mentioned in the discussion of Figure 3 and as known from previous studies,[5,7,14,15] the fast relaxation time increases with increasing laser pump power for the gold nanodots in solution as well as for the particles in $MgSO_4$ powder. The same is true for the slow decay component. While the latter appears to be of comparable magnitude for the two samples (Figure 5b), the fast relaxation time is considerably longer for the particles in $MgSO_4$ powder compared to particles in solution (Figure 5a). An extrapolation to zero pump power would lead to the same conclusion. However, the extrapolation procedure is complicated by the fact that different values for the limiting relaxation time at zero pump power are found, depending on the specific range of excitation energies for which the extrapolation is carried out. The reason for this is that a linear dependence of the relaxation times as a function of excitation power is only observed at very low pump intensities. At higher pump intensities, the relaxation times reach a plateau. This fact is slightly buried by the representation in Figure 5 since a logarithmic scale for the x-axis is used in order to show all the measured relaxation times in a more dispersed way. Therefore, different limiting decay times can easily be obtained by this procedure, and the question of a lower sensitivity for the diffuse reflectance measurements could be raised again.

Plotting the decay times against the absorbed laser energy instead of the total laser energy would be the solution, which might be achieved in an indirect way. Figure 5c shows how the amplitude ratio between the two decay components increases with increasing laser pump power. The value for the amplitude ratio was simply determined by dividing the bleach intensity at 50 ps by the maximum bleach intensity at ~0 ps. The bleach is due to the hot electrons, and the total intensity will depend on the laser pump power as well as on the sample concentration and the optical path length as discussed above. However, the amplitude ratio taken at 50 ps should correspond to the relative temperature of the electrons while being in equilibrium with the lattice and possibly in partial equilibrium with the surrounding medium (see discussion below). By taking this intensity ratio, one obtains a relative value, which is no longer dependent on the experimental parameters and hence represents a way of measuring the internal temperature of the particles. The decay times from Figure 5a,b are therefore plotted against their relative

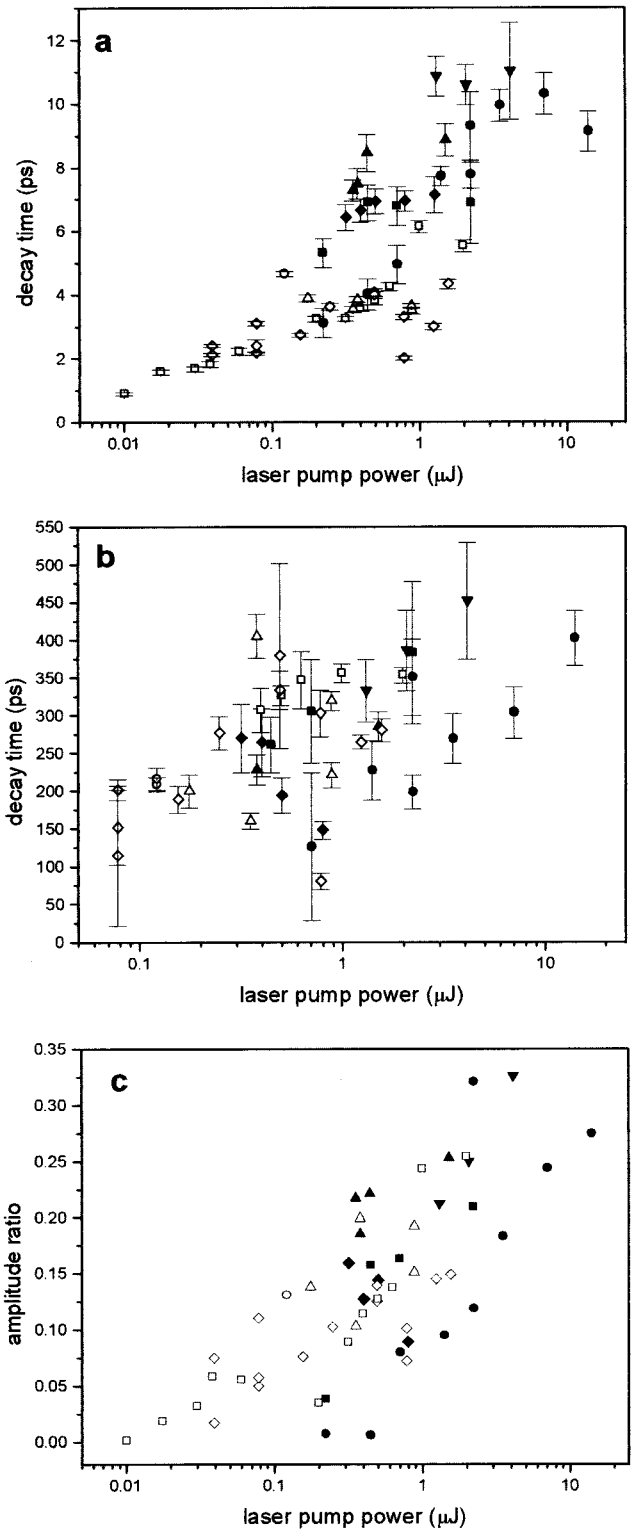

Figure 5. Plots of the fast (a) and slow (b) decay components of the plasmon band bleach as a function of exposed laser pump power. The open (closed) symbols were measured for the gold nanodots in solution ($MgSO_4$ powder). The decay components and their error bars were obtained by fitting the experimental data to a biexponential function. The different symbols represent measurements carried out on several days in order to test the reproducibility of the results and to cover a large range of excitation energies. (Note the logarithmic scale.) In summary, both decay times increase with increasing pump power. This is also the case for the relative amplitude ratio of the fast to the slow decay component as shown in panel c. The value for the amplitude ratio was simply determined by dividing the bleach intensity at 50 ps by the maximum bleach intensity at ~0 ps.

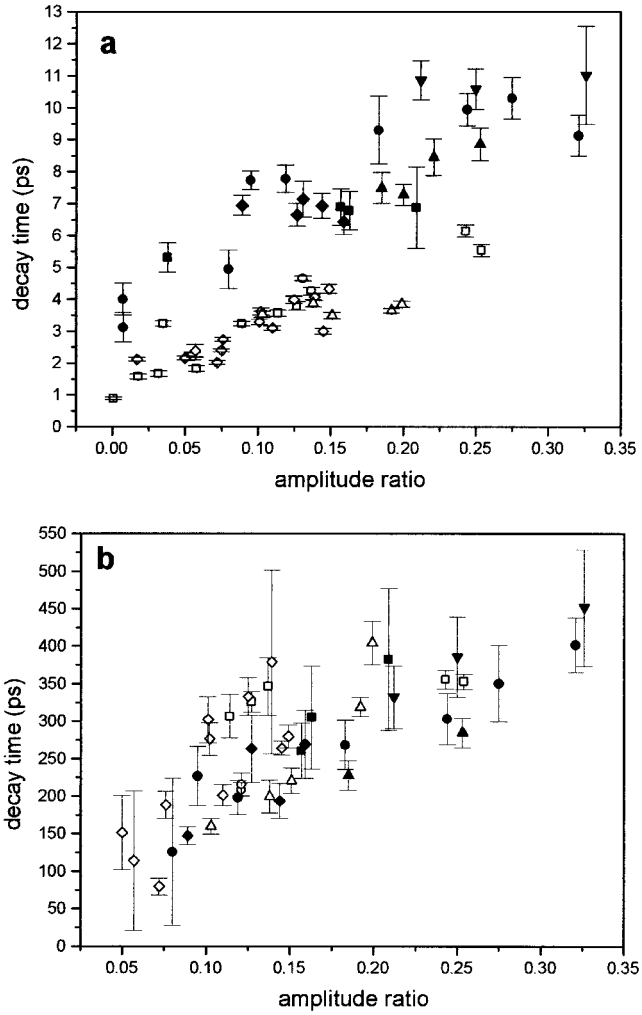

Figure 6. Plots of the fast (a) and slow (b) decay components of the plasmon band bleach as a function of the relative amplitude ratio. The open (closed) symbols were measured for the gold nanodots in solution ($MgSO_4$ powder). Since the bleach signal of the gold nanodots is due to an increase in the electron temperature and because electrons and the lattice have equilibrated thermally within 50 ps, the amplitude ratio is a direct measure for the actual temperature of the particles and hence a measure of the absorbed laser energy rather than the total pulse energy. Following this argumentation, the data presented in Figure 5a,b has been normalized by plotting the decay times against the amplitude ratio (or an effective internal temperature). This procedure eliminates especially the fluctuations seen by carrying out these measurements on different days adding to the validity of this representation.

amplitude ratios as shown in Figure 6a,b for the fast and slow decay components, respectively. This procedure reduces the scatter of the data points between the measurements taken on different days, which are represented by different symbols. This indicates that the proposed analysis is justified since it eliminates the problems associated with slightly different excitation conditions on different days. For example, a slightly different overlap between the pump and probe beams can lead to different results as the gold nanoparticles are heated more effectively in the center of the excitation beam. Figure 6 shows that the fast relaxation time is about twice as long for the gold particles embedded in $MgSO_4$ powder compared to the nanodots in solution while the slow relaxation time is very comparable for the two media considering the associated error bars. This comparison assumes that the heat capacities of the two systems are comparable so that the equilibrium temperatures after 50 ps are indeed similar. Since the gold nanodot-$MgSO_4$ composite

powder contains also air, it is difficult to estimate if this assumption is indeed correct. A strong argument confirming the results in Figure 6 will, however, be made in the following section.

D. Effect of Adding Solvent to the Gold Nanodot−$MgSO_4$ Composite. We performed another experiment in order to prove that the difference in the bleach relaxation dynamics of the gold nanoparticles in different media is indeed real and not caused entirely by the two different spectroscopic techniques used (reflectance vs transmission spectroscopy) and possible different excitation conditions (different amounts of absorbed laser energy). Using the same optical setup for measuring the transient diffuse reflectance, gold nanodots in $MgSO_4$ powder were measured, and then this experiment was repeated under identical conditions after adding THF to the sample. The THF replaced the air surrounding the particles, which was clearly visible as bubbles streamed through an upper liquid layer on top of the $MgSO_4$ powder. The results of this experiment are shown in Figure 7a, which gives the plasmon bleach recovery of 14.5 nm spherical gold nanoparticles embedded in $MgSO_4$ powder (solid squares) and after adding THF to the sample (open spheres). Excitation was carried out at 400 nm with an excitation power of 2.70 μJ and the probe wavelength was set to 540 nm recording the changes in the transient diffuse reflectance in both cases. While the fast decay component decreases by about a factor of 2 from 9.50 to 5.71 ps upon the addition of the solvent, the slow components are very much comparable considering the experimental error. This is more clearly seen in the inset, which shows the dynamics of the plasmon bleach recovery on a shorter time scale. A decrease of the fast relaxation time by a factor of 2 is very similar to the conclusions drawn from Figure 6, which therefore supports the evaluation chosen above.

Experimentally, we observed a decrease in the reflected light intensity after adding THF to the gold particles in $MgSO_4$ powder. This could be due to an increase in the absorption coefficient K combined with a decrease of the scattering coefficient *S* (see eq 1). Generally, the scattering coefficient becomes small when air is replaced with solvent because the reflectivity at the interface between the particles and the medium decreases due to a smaller difference in the refractive indices. An increase in the absorption coefficient would lead to a larger amount of laser energy absorbed by the gold nanoparticles after the addition of THF. However, from the known power dependence of the two decay components (see Figure 5a,b) an increase of both relaxation times is expected for the sample with the solvent added if the absorption coefficient increases. This is not observed experimentally. Therefore, it can be assumed that the excitation conditions are only slightly changed after the addition of THF and do not affect the main result that mainly the fast relaxation component is accelerated.

A similar result is also obtained in an experiment shown in Figure 7b. Instead of adding solvent to the $MgSO_4$ powder, the powder containing the gold nanoparticles was compressed in an IR pellet die and then measured by transient diffuse reflectance spectroscopy. By compressing the powder better contact between the powder and the particles was established eliminating part of the air around the particles. As a consequence, the fast decay component decreases from 11.38 to 6.28 ps for the compressed sample (open spheres) as compared to that for the uncompressed sample (solid squares). These results clearly demonstrate that the fast decay component changes with the environment.

IV. Discussion

The observation that the fast decay component previously ascribed to the electron−phonon relaxation inside the gold nanoparticles depends on the environment of the particles was rather unexpected. It was thought that the slow decay component ascribed to the phonon−phonon relaxation between the particles and the surrounding medium should be changed. These results therefore raise the question of whether the assignment of the two decay components to the electron−phonon and phonon−phonon interactions is entirely correct. If the fast relaxation corresponds to just the coupling between electrons and lattice phonons of the metal particle, then this should be independent of the particle's environment. Therefore, it might be necessary to distinguish further between the transfer of heat from the gold nanoparticles to the close environment and then the subsequent heat conduction away from the direct vicinity of the particles leading to thermal equilibration of the whole sample. If it is assumed that the heat exchange with a small layer of the medium around the particles is also represented by the fast decay component and the second component corresponds to the heat conduction within the host medium, then these results could be understood. The longer relaxation times measured for the particles embedded in $MgSO_4$ powder are then due to a hindered heat exchange between the metallic particles and the inorganic salt especially since most of the interface is believed to consist of air. On the other hand, in the low perturbation regime using lower excitation energies, the heat exchange and transfer with the matrix are less important since the temperature change for the metallic nanoparticles is only on the order of a few degrees. The fast relaxation time then corresponds to pure electron−phonon interactions inside the nanoparticles. Basically, it becomes a questions as to which process in the cooling dynamics of the metal nanoparticles (electron−lattice coupling inside the gold particles, heat transfer between the gold particles and the medium, and thermal equilibration of the medium by heat conduction) is the rate-limiting step for particles in different media with different thermal (heat capacity, heat conductivity) as well as physical properties (contact area, physiosorption, chemisorption of the surrounding molecules) at different levels of excitation/heating.

In the experiments presented here, the electron−phonon relaxation process in the dots needs to involve phonons at the interface in order to explain the results. The coupling with the vibrations of the surrounding medium could contribute greatly to the heat sink needed to cool off the hot electrons. Since the electron charge density of the conduction band wave functions can extend beyond the physical boundaries of the nanoparticles (electron spill out effect[32]), it could be possible that the electrons of the gold particle can directly couple to the vibrational modes of the molecules attached to the surface of the gold nanodots. Furthermore, a model known as chemical interface damping[36] correlates the plasmon bandwidth to the nature of the surrounding medium by assuming that electrons can undergo a charge transfer into an unoccupied orbital of an adsorbed molecule at the particle interface. After subsequent back electron transfer, the initial phase of the electrons induced by the plasmon excitation will be lost. A faster dephasing time will lead to a broadening of the plasmon band, which is indeed seen if the same particles are embedded in a solid medium compared to vacuum.[37] This model only assumes the loss of phase. However, if the back electron transfer does not occur from the same orbital but after electronic relaxation by coupling to the vibrational modes of the adsorbed molecule, part of the absorbed laser

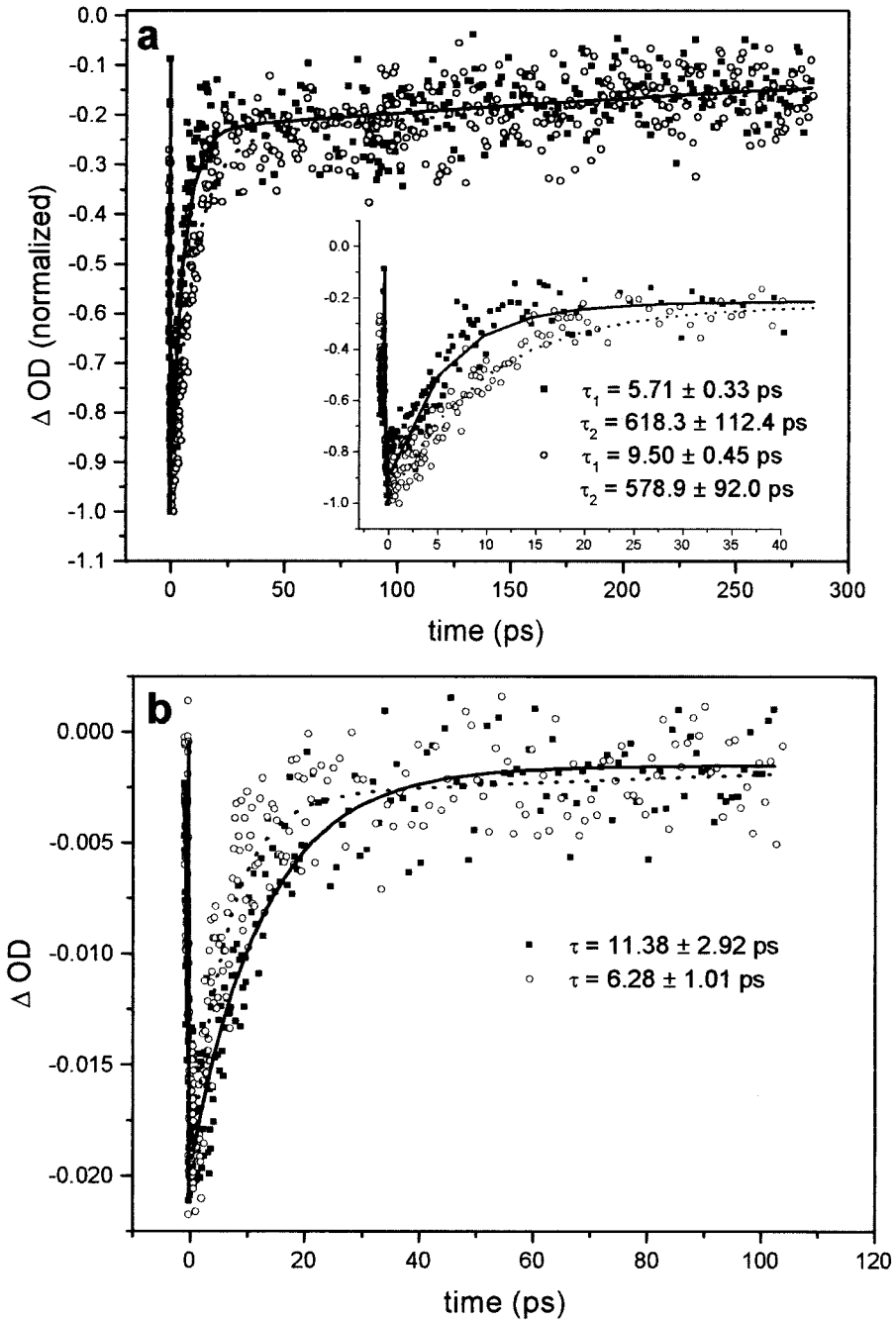

Figure 7. (a) Plasmon bleach recovery of 14.5 nm spherical gold nanoparticles embedded in $MgSO_4$ powder (solid squares) and after adding THF to the sample (open spheres). Excitation was carried out at 400 nm, and the probe wavelength was set to 540 nm recording the changes in the transient diffuse reflectance in both cases. The excitation power was 2.70 μJ, and the kinetic traces have been normalized for better comparison. While the value for the fast decay component decreases from 9.50 to 5.71 ps upon the addition of the solvent, the slow component is of comparable magnitude considering the error. This is more clearly seen in the inset, which shows the dynamics of the plasmon bleach recovery on a shorter time scale. The added solvent replaced the air surrounding the particles (which could actually be seen in form of bubbles) and enabled a better heat exchange between the gold nanodots and their surrounding. (b) Plasmon bleach recovery of 14.5 nm spherical gold nanoparticles embedded in $MgSO_4$ powder (solid squares) and after physical compression of the powder (open spheres). Excitation was carried out at 400 nm, and the probe wavelength was set to 540 nm recording the changes in the transient diffuse reflectance. The excitation power was 1.35 μJ, and the kinetic traces have been normalized for better comparison. An acceleration of the plasmon bleach recovery is again seen in the fast decay component, as in this experiment the air is partly replaced by a more compact $MgSO_4$ powder.

energy will be directly transferred to the molecules, which are in close contact with the metal nanoparticle.

The fact that similar decay times are obtained for the slow component might suggest that (1) the heat conductivity in both media is comparable (which is hard to estimate quantitatively since the particles are also surrounded by air and not only $MgSO_4$ powder in case of the solid sample) or that (2) the environment represents such a large heat sink (reservoir) in comparison with the small excitation area that a possible difference in the relaxation dynamics is not observed.

It is, however, also possible that the quantized phonon spectrum inside the gold nanoparticles could be affected by the nature of the surrounding medium. This could possibly produce a phonon bottleneck for particles, which are mainly surrounded by air and then lead to a reduced electron−phonon relaxation. This explanation is also consistent with our observed results

and does not involve the excitation of molecular vibration of the surrounding molecules within the first few picoseconds. However, eventually the absorbed light energy will have to be transferred to the surrounding matrix and more experiments might be necessary to find out on which time scale this latter process actually takes place.

In summary, the experiments presented strongly suggest a change in the relaxation dynamics when gold nanodots are transferred from the solution phase to an inorganic salt. The medium therefore plays an important role in the cooling of the nanoparticles. A similar effect was also observed by Bigot et al.,[18] who measured the relaxation dynamics of 6.5 nm silver nanoparticles embedded in two different types of transparent glasses (alumina and glass). They also found an increase of the electron−phonon relaxation time from 0.77 to 1.4 ps when comparing the alumina and glass matrixes, respectively. They explained their results in terms of the better heat conductivity of the alumina. However, the heat conductivity of a dielectric film is much higher than that of a solution, and since these authors were working in the low excitation regime, they did not observe a second longer decay component. On the other hand, Zhang and co-workers[13] reported a reduction of the electron−phonon relaxation time from 7 to 3.5 ps for 15 nm gold nanoparticles when the solvent was changed from water to cyclohexane. However, on the basis of the higher heat conductivity of water compared to organic solvents, one would expect the opposite behavior in this case. This might suggest that other factors such as the specific chemical nature of the particle interface (e.g., capping material for colloidal nanoparticles) are of importance, which may not be expressed by only a bulk thermodynamic value. We were recently able to incorporate chemically prepared gold nanoparticles into a polymer hydrogel and then exchange the water with organic solvents.[38] It was found that both decay components depend on the surrounding medium as they increase by a change from water to hydrogel and then to an organic gel. It was therefore concluded that the electron relaxation dynamics depend on the thermal properties, chemical structure, and molecular dynamics of the surrounding medium. These results agree well with the current study presented here although more work on the specific nature of the coupling between metal nanoparticles and their surrounding is still needed in order to give a more complete picture for the origin of the slow decay component observed in the plasmon band bleach at higher laser excitation powers.

Acknowledgment. This research was supported by the National Science Foundation (Grant No. CHE 9705164). A. Furube is a research fellow of the Japanese Society for the Promotion of Science, and M. B. Mohamed would like to thank Egyptian GM for a Ph.D. fellowship. H. Masuhara thanks the Grant-in-Aid on Priority Area (B) on "Laser Chemistry of Single Nanometer Organic Particles" (10207204) from the Ministry of Education, Science, Sports, and Culture for the financial support.

References and Notes

(1) Hamanaka, Y.; Hayashi, N.; Nakamura, A.; Omi, S. *J. Lumin.* **1998**, *76&77*, 221.
(2) Perner, M.; Bost, P.; v. Plessen, G.; Feldmann, J.; Becker, U.; Mennig, M.; Schmidt, H. *Phys. Rev. Lett.* **1997**, *78*, 2192.
(3) Perner, M.; Klar, T.; Grosse, S.; Lemmer, U.; v. Plessen, G.; Spirkl, W.; Feldmann, J. *J. Lumin.* **1998**, *76&77*, 181.
(4) Inouye, H.; Tanaka, K.; Tanahashi, I.; Hirao, K. *Phys. Rev. B* **1998**, *57*, 11334.
(5) Ahmadi, T. S.; Logunov, S. L.; El-Sayed, M. A. *J. Phys. Chem.* **1996**, *100*, 8053.
(6) Ahmadi, T. S.; Logunov, S. L.; El-Sayed, M. A.; Khoury, J. T.; Whetten, R. L. *J. Phys. Chem. B* **1997**, *101*, 3713.
(7) Link, S.; Burda, C.; Wang, Z. L.; El-Sayed, M. A. *J. Chem. Phys.* **1999**, *111*, 1255.
(8) Link, S.; Burda, C.; Mohamed, M. B.; Nikoobakht, B.; El-Sayed, M. A. *Phys. Rev. B* **2000**, 61, 6086.
(9) Link, S.; El-Sayed, M. A. *J. Phys. Chem. B* **1999**, *103*, 8410.
(10) Smith, B. A.; Waters, D. M.; Faulhaber, A. E.; Kreger, M. A.; Roberti, T. W.; Zhang, J. Z. *J. Sol.-Gel Sci. Technol.* **1997**, *9*, 125.
(11) Faulhaber, A. E.; Smith, B. A.; Andersen, J. K.; Zhang, J. Z. *Mol. Cryst. Liq. Cryst.* **1996**, *283*, 25.
(12) Smith, B. A.; Zhang, J. Z.; Giebel, U.; Schmid, G. *Chem. Phys. Lett.* **1997**, *270*, 139.
(13) Zhang, J. Z. *Acc. Chem. Res.* **1997**, *30*, 423.
(14) Hodak, J. K.; Martini, I.; Hartland, G. V. *Chem. Phys. Lett.* **1998**, *284*, 135.
(15) Hodak, J. K.; Martini, I.; Hartland, G. V. *J. Phys. Chem. B* **1998**, *102*, 6958.
(16) Hodak, J. K.; Henglein, A.; Hartland, G. V. *J. Chem. Phys.* **1999**, *111*, 8613.
(17) Bigot, J.-Y.; Merle, J.-C.; Cregut, O.; Daunois, A. *Phys. Rev. Lett.* **1995**, **75**, 4702.
(18) Halte, V.; Bigot, J.-Y.; Palpant, B.; Broyer, M.; Prevel, B.; Perez, A. *Appl. Phys. Lett.* **1999**, *75*, 3799.
(19) Bigot, J.-Y.; Halte, V.; Merle, J.-C.; Daunois, A. *Chem. Phys.* **2000**, **251**, 181.
(20) Del Fatti, N.; Vallee, F.; Flytzanis, C.; Hamanaka, Y.; Nakamura, A. *Chem. Phys.* **2000**, *251*, 215.
(21) Del Fatti, N.; Tzortzakis, S.; Voisin, C.; Flytzanis, C.; Vallee, F. *Phys. B* **1999**, *263−264*, 54.
(22) Del Fatti, N.; Voisin, C.; Chevy, F.; Vallee, F.; Flytzanis, C. *J. Chem. Phys.* **1999**, *110*, 484.
(23) Del Fatti, N.; Flytzanis, C.; Vallee, F. *Appl. Phys. B* **1999**, *68*, 433.
(24) Stagira, S.; Nisoli, M.; De Silvestri, S.; Stella, A.; Tognini, P.; Cheyssac, P.; Kofman, R. *Chem. Phys.* **2000**, *251*, 259.
(25) Stella, A.; Nisoli, M.; De Silvestri, S.; Svelto, O.; Lanzani, G.; Cheyssac, P.; Kofman, R. *Phys. Rev. B* **1996**, *53*, 15497.
(26) Nisoli, M.; Stagira, S.; De Silvestri, S.; Stella, A.; Tognini, P.; Cheyssac, P.; Kofman, R. *Phys. Rev. Lett.* **1997**, *53*, 3575.
(27) Reetz, M. T.; Helbig, W. *J. Am. Chem. Soc.* **1994**, *116*, 7401.
(28) Reetz, M. T.; Helbig, W.; Stimming, U.; Breuer N.; Vogel, R. *Science* **1995**, *267*, 367.
(29) Reetz, M. T.; Helbig, W.; Quaiser, S. A. *Chem. Mater.* **1995**, *7*, 2227.
(30) Asahi, T.; Furube, A.; Fukumura, H.; Ichikawa, M.; Masuhara, H. *Rev. Sci. Instrum.* **1998**, *69*, 361.
(31) Furube, A.; Asahi, T.; Masuhara, H.; Yamashita, H.; Anpo, M. *J. Phys. Chem. B* **1999**, *103*, 3120.
(32) Kreibig, U.; Vollmer, M. *Optical Properties of Metal Clusters*; Springer: Berlin, 1995.
(33) Kerker, M. *The Scattering of Light and Other Electromagnetic Radiation*; Academic Press: New York, 1969.
(34) Bohren, C. F.; Huffman, D. R. *Absorption and Scattering of Light by Small Particles*; John Wiley: New York, 1983.
(35) Johnson, P. B.; Christy, R. W. *Phys. Rev. B* **1972**, *6*, 4370.
(36) Persson, N. J. *Surf. Sci.* **1993**, *281*, 153.
(37) Hoevel, H.; Fritz, S.; Hilger, A.; Kreibig, U.; Vollmer, M. *Phys. Rev. B* 1993, *48*, 18178.
(38) Mohamed, M. B.; Ahmadi, T. S.; Link, S.; Braun, M.; El-Sayed, M. A. *Chem. Phys. Lett.* **2001**, *343*, 55.